Geosci. Instrum. Method. Data Syst. Discuss., https://doi.org/10.5194/gi-2019-13
Manuscript under review for journal Geosci. Instrum. Method. Data Syst.
Discussion started: 8 May 2019

Geoscientific Instrumentation Methods and Data Systems Discussions
Open Access

Evaluations of an ocean bottom electro-magnetometer and preliminary results offshore NE Taiwan

Ching-Ren Lin[1], Chih-Wen Chiang[2], Kuei-Yi Huang[2], Yu-Hung Hsiao[3], Po-Chi Chen[3], Hsu-Kuang Chang[3], Jia-Pu Jang[3], Kun-Hui Chang[1], Feng-Sheng Lin[1], Saulwood Lin[4], and Ban-Yuan Kuo[1]

1 Institute of Earth Sciences, Academia Sinica, Taipei 11529, Taiwan, R.O.C

2 Institute of Earth Sciences, National Taiwan Ocean University. Keelung 20224, Taiwan, ROC.

3 Taiwan Ocean Research Institute, National Applied Research Laboratories, Kaohsiung 80143, Taiwan, R.O.C.

4 Institute of Oceanography, National Taiwan University, Taipei 10617, Taiwan, R.O.C

Corresponding author: Chih-Wen Chiang

Address: Institute of Earth Sciences, National Taiwan Ocean University, Keelung 20224, Taiwan

E-mail: zjiang@ntou.edu.tw

Tel: +886-2-24622192 Ext.6513

Fax: +886-2-24625038

April, 2019

ABSTRACT

The first stage of field experiments involving the design and construction of a low-power consumption ocean bottom electro-magnetometer (OBEM) has been completed. To improve the performance of the OBEM, we rigorously evaluated each of its units, e.g., the data loggers, acoustic parts, internal wirings, and magnetic and electric sensors, to eliminate unwanted events such as unrecovered or incomplete data. The evaluations of the procedure included the following.

- Data logger: digitizer sensitivity, linearity, and errors
- Acoustic transceiver: “ENABLE,” “DISABLE,” “RANGE,” “RELEASE1,” “RELEASE2,” and “OPTION1” functions
- Magnetic sensor: sensitivity of the fluxgate and orthogonality
- Electrical receiver: potential voltage, impedance, and frequency responses
- Power consumption: the maximum operating current of two sets of batteries
- Deployment and recovery procedures on deck

We confirmed the optimal performance of the OBEM after repeatedly testing the procedures.

The first offshore deployment of the OBEM together with ocean bottom seismographs (OBSs) was performed in NE Taiwan, where the water depth is approximately 1,400 m. The total intensity of the magnetic field (TMF) measured by the OBEM varied in the range of 44,100–44,150 nT, which corresponded to the proton magnetometer measurements. The daily variations of the magnetic field were recorded using the two horizontal components of the OBEM magnetic sensor. We found that the inclinations and magnetic data of the OBEM varied with two observed earthquakes when compared to the OBS data. The potential fields of the OBEM were slightly, but not obviously, affected by the earthquakes.

Keywords: OBEM; data logger; acoustic transceiver; fluxgate; non-polarizing electrodes.

1. Introduction

Marine electromagnetic exploration is a geophysical prospecting technique used to reveal the electrical resistivity features of the oceanic upper mantle down to depths of several hundreds of kilometers in different geologic and tectonic environments, such as in areas around mid-oceanic ridges, areas around hot-spot volcanoes, subduction zones, and normal ocean areas between mid-oceanic ridges and subduction zones zones (Ellis et al., 2008; Evans et al., 2005; Key, 2012; Utada, 2015). Marine controlled source electromagnetic (MCSEM) methods have been used for methane hydrate mapping to detect offshore hydrocarbons (Constable, 2010; Goto et al., 2008; Schwalenberg et al., 2017; Weitemeyer et al., 2011; Weitemeyer et al., 2006).

Even though many magnetotelluric explorations have investigated deep electrical structures on Taiwan (Bertrand et al., 2009; Bertrand et al., 2012; Chiang et al., 2011a; Chiang et al., 2010; Chiang et al., 2015; Chiang et al., 2008), there were no marine electromagnetic experiments around Taiwan until 2010. The first MCSEM survey was carried out for gas hydrate investigations offshore SW Taiwan (Hsu et al., 2014). Marine electromagnetic methods have gradually gained the attention of Taiwanese scientists following these MCSEM experiments (Chiang et al., 2012; Chiang et al., 2011b).

The first generation of ocean bottom seismographs (OBSs) was developed by the Institute of Earth Sciences, Academia Sinica (IES), Taiwan Ocean Institute, National Applied Research Laboratories, and the Institute of Undersea Technology, National Sun Yat-sen University (OBS R&D team), in 2009, the so-called Yardbird-20s. These OBSs have acquired large amounts of data via a series of deployments offshore Taiwan that can be used to study plate tectonics and crustal characteristics (Kuo et al., 2015; Kuo et al., 2012; Kuo et al., 2014). Subsequently, the OBS R&D team developed an ocean bottom electro-magnetometer (OBEM) modified from the OBS based on important developmental experiments.

The novel OBEM was constructed by the OBS R&D team and has completed the first stage of field experiments by the Institute of Earth Sciences, National Ocean Taiwan University, and IES. One OBEM and six broadband OBSs, so-called BBYBs, were deployed at the western end of the Okinawa Trough (OT), NE Taiwan, for field testing in March 2018. The water depth in this area is approximately 1,400 m. All the instruments were successfully recovered in May 2018 after collecting the first OBEM field data in Taiwan. Here, we introduce the OBEM design, specifications, calibration procedures, and its further developments and improvements.

2. The OBEM design

The OBEM is designed to be wireless deep-underwater equipment; however, the power supply is limited for the wireless OBEM because the batteries cannot be directly charged via electric cables from vessels. Therefore, designing low-power consumption for the OBEM and high-efficiency battery packs is critically required for long periods of operation. The major units of the OBEM include a data logger, a magnetic sensor, a tiltmeter, electric receivers with an arm-folding mechanism, a relocation system, recovery units, and an anchor. All the units for the OBEM use nonmagnetic materials (e.g., the screws and anchor). Figure 1 shows a block diagram of the OBEM. We designed the data logger, release mechanism, and the OBEM platform to integrate all the sensors or units purchased from related manufactories and focused on the issues of saving power and reducing costs. The detailed requirements of the OBEM are listed below.

1. A magnetic sensor with three axes for measuring magnetic fields
2. A tiltmeter with two axes for measuring leveling changes to correct the tilt error of the magnetic sensor
3. Two pairs of non-polarized electrodes with 2-m bendable arms with a total distance between the electrodes of approximately 4.5 m
4. A highly accurate data logger with at least seven channels and a sampling rate of greater than or equal to 10 samples per second (SPS)
5. An operation time of more than 90 days
6. An internal timing error of less than 3 s y^{-1} synchronized with GPS
7. Acoustic relocation and recovery control systems
8. A power consumption of less than 1.5 W
9. A radio beacon, flush beacon, reflect label, and orange flag for identification on the sea surface during instrument recovery
10. A 0.75 m s^{-1} subside rate for deployment and float up rate for recovery
11. A maximum deployment depth of more than 6,000 m appropriate for most seawater depths offshore Taiwan

The solutions found for the OBEMs are listed below.

1. A fluxgate with three axes with a sensitivity of ±70,000 nT
2. A tiltmeter with two axes with inclinations of ±30°
3. Two pairs of silver chloride electrodes with a 2-m arm-folding mechanism
4. A low noise and low-power consumption eight differential channel 24-bit A/D data logger with an accurate internal timing clock
5. Acoustic transponder and controller units
6. Radio beacon and flash beacon units
7. An OBEM platform modified from that of OBS
8. High-efficiency lithium battery packs for the sensors and data logger

3. Units of the OBEM and their specifications

The OBEM is recovered by releasing its anchor from the seafloor via an on-board acoustic command. The OBEM is returned to the sea surface via buoyancy when the anchor is released. There are two typical release mechanisms available for OBEMs to unlock their anchors: spin motor and burn-wire systems (Kasaya and Goto, 2009). The OBEM uses the burn-wire system because it weighs less than the spin motor system. The acoustic controller and transducer use ORE #B980175 ASSY PCB and #D980709, respectively, manufactured by EdgeTech, USA, for the corresponding functions of OBEM recovery and underwater ranging. The ASSY PCB acoustic controller uses a binary FSK encoder, including the commands “RELEASE1,” “RELEASE2,” “DISABLE,” “ENABLE,” and “OPTIONAL1.” The frequency of the acoustic range ranges from 7.5 kHz to 15 kHz in increments of 0.5 kHz with a sensitivity of 80 dB re 1uPa. The #D980709 transducer can work at a depth of 6,000 m and in environments from −10°C to +40°C.

The EdgeTech 8011M model acoustic commander (8011M) is used on board to send the “ENABLE” command to open the ranging function, the “RANGE” command to measure the distance between the OBEM and the research vessel, the “DISABLE” command to close the ranging function, and the “RELEASE1” command to activate the burn-wire system to release the anchor. The “RELEASE1” command persists for 15 min unless terminated by the “OPTIONAL1” command.

We selected the RF-700A and ST-400A NOVATECH models for the radio and flash beacons, respectively, for use in the OBEM. The maximum deployment depth for these models is 7,300 m. The radio beacon is turned ON by sending a VHF signal, and the flush beacon is turned ON at an atmospheric pressure of less than 1 atm (equal to a depth of 10 m below the sea surface) in a dark environment. The beacons are also turned OFF at a depth of 10 m or at an atmospheric pressure of less than 1 atm, respectively. These two beacons have four independently installed C-type alkaline batteries that allow for six days of continuous operation at maximum; this power supply differs from that of the data logger. The two independent power supply layouts allow the beacons to properly operate even if the power supply for the data logger fails. An on-board radio scanner detects the signal transmitted from the radio beacon at a distance of 6.4–12.9 km when the OBEM is floating on the surface. These two beacons can assist in locating the OBEM on the sea surface in both daytime and nighttime.

TL-5930 model lithium batteries manufactured by TADIRAN are used for the OBEM, with specifications of 3.6 V, 19 Ah, and D-type with characteristics of high energy density and a low self-discharge rate suitable for long periods of operation. Figure 2 shows a block diagram of the OBEM data logger. The ADC1278EVM model is a 24-bit A/D converter used for the inputs of the three fluxgate axes, the two tiltmeter axes, and two pairs of non-polarized electrodes with a sampling rate of 10 SPS. An amplifier and low-pass filter (Amp & LPF) were designed for the magnetic sensor, leveling sensor, and electric receiver inputs. The two MPS430F5436A microcontrollers (MCU) process the timing synchronization of the time base manufactured by SeaSCAN, USA, and the GPS modules; the digital data is stored to a Secure Digital (SD) memory card with a standard Secure Digital High Capacity (SDHC), and the user interface communicates with a PC. The time base module supplies a precise time base signal to the data logger, whereas the SISMTB Ver 4.1 time base module generates a precise 125-Hz clock that supports a timing error smaller than 3 s y^{-1}. Even though the time base module supports a very small timing error of 3 s y^{-1}, the data logger clock is still synchronized with the GPS on deck for timing corrections after recovering the OBEM. The maximal capacity of the SD card is 64 GB and can support data storage for more than one year with a sampling rate of 10 SPS.

Two 17-in glass VITROVEX spheres manufactured by Nautilus Marine Service GmbH, Germany, are used for the OBEM. These glass spheres contain the fluxgate and tiltmeter (sensor ball) and the seven channels of the Amp & LPF, data logger, #B980175 ASSY PCB acoustic controller, and batteries (instrument ball) and can be deployed at a depth of 6,000 m and support a total buoyancy of 52 kg. The instrument and sensor balls, the silver chloride electrodes, and the burn-wire system are connected via waterproof cables. There is a pressure-vacuum valve outside the glass spheres that allows a pumped vacuum to be preserved at 0.7 atm; self-fusing butyl rubber tape is used to fill the suture zone between the half glass spheres. In addition, two crossed stainless-steel bands are used to improve the waterproofing of the glass spheres and cover the orange PE cases. Four PVC pipes with lengths of 2 m are combined to form the OBEM platform for the electric receivers, and the silver chloride electrodes are installed at the ends of the pipes. A 60-kg nonmagnetic anchor is attached to the bottom of the OBEM platform and catches via a releasing mechanism. The anchor can be released using the burning-wire system to recover the OBEM. Figure 3 shows a photograph of the OBEM platform.

4. Calibrations of the OBEM

It is necessary to calibrate each unit of the OBEM, including the data logger with the Amp & LPF, fluxgate, tiltmeter, electrodes, ASSY PCB acoustic controller, transducer, and wiring, before and after assembling the OBEM to improve its performance. We describe the series of calibration methods used for the OBEM units in the following section.

4.1 Calibrations of the background noise of the data logger and the Amp & LPF

The background noise of the data logger is defined as

$$N_{rms} = \sqrt{\frac{1}{n}(A_1^2 + A_2^2 + \cdots + A_n^2)}, (1)$$

where n is a data point and A_1 to A_n indicate the amplitudes of the data points, 1 to n, individually at short circuit or 0 V. The background noise of the data logger (in "BIT") is calculated as

$$dB_{rms} = 20\, log_2(N_{rms}), \quad (2)$$

The data logger contains seven input channels called MX, MY, MZ, TX, TY, EX, and EY. MX, MY, and MZ are used for the magnetic sensor of the fluxgate, TX and TY are used for the tiltmeter, and EX and EY are used for the electric receivers. The calibration procedure is described below.

1. Connect MX, MY, MZ, TX, and TY to GND, EX+ with EX−, and EY+ with EY−.
2. Start the record mode of the data logger, wait 60 s to acquire data, and then stop recording data.
3. Download the data from the data logger and convert it to ASCII format. Then, calculate the background noise using Eq. (1) and the background noise in dB using Eq. (2).

4.2 Calibrations of the sensitivity, linearity error, and dynamic range for the data logger and the Amp & LPF

The input ranges of the voltages for MX, MY, and MZ are ±10 V, for TX and TY are ±5 V, and for EX and EY are ±0.00625 V. The sensitivities are calculated from the average count of the input voltages, that is, subtract the average count at zero voltage and then divide by the input voltages:

$$S = Average\left(\frac{Average(C_i)-Average(C_0)}{V_i}\right), \quad (3)$$

where V_i is the input voltage, C_i is the output count saved on the SD card for an input voltage of V_i, and C_0 is the output count saved on the SD card for an input voltage of 0 V.

The linearity errors are calculated such that

$$Error = Abs\left[\frac{S_i-S_T}{S_T}\right] \times 100, \quad (4)$$

where S_i is the sensitivity of the input voltage and S_T is the total sensitivity.

The dynamic range is the ratio of the maximum count to the background noise. It is defined as

$$D = 20\,log\left(\frac{S_T \times V\,max}{N_{RMS}}\right), (5)$$

where S_T is the total sensitivity and Vmax is 10 V for MX, MY, and MZ, 5 V for TX

Geosci. Instrum. Method. Data Syst. Discuss., https://doi.org/10.5194/gi-2019-13
Manuscript under review for journal Geosci. Instrum. Method. Data Syst.
Discussion started: 8 May 2019

Geoscientific Instrumentation Methods and Data Systems
Discussions
Open Access

and TY, and 0.00625 V for EX and EY. Its calibration procedure is described below.

1. Connect the MX, MY, and MZ channels of the data logger to the source voltages generated by the calibrator (FLUKE726) and connect the GND channel of the data logger to the source common point (COM) of FLUKE726.
2. Set the data logger to the recording mode.
3. Set the FLUKE726 output voltages from 0 V to ±10 V. Increase and decrease the voltages step by step in 1 V intervals until ±10 V. The measurement time length for each output voltage is 20 s.
4. Connect the TX and TY channels of the data logger to the source voltages generated by FLUKE726 and connect the GND channel of the data logger to COM of FLUKE726.
5. Set the FLUKE726 output voltages from 0 V to ±5 V. Increase and decrease the voltages step by step in 1 V intervals until ±5 V. The measurement time length for each output voltage is 20 s.
6. Connect the EX+ and EY+ channels of the data logger to the source voltages generated by FLUKE726, and connect the EX− and EY− channels of the data logger to COM of FLUKE726.
7. Set the FLUKE726 output voltages from 0 V to ±6 mV. Increase and decrease the voltages step by step in 1-mV intervals until ±6 mV. The measurement time length for each output voltage is 20 s.
8. Finally, switch off the recording mode of the data logger, download the data, and convert it to ASCII format for analysis. Calculate the sensitivity, linearity error, and dynamic range using Eqs. (3), (4), and (5), respectively.

Tables 1–3 show the results for the background noise, sensitivity, linearity error, and dynamic range of the calibrations of the magnetic (MX, MY, and MZ), electric (EX and EY), and tiltmeter (TX and TY) channels of the OBEM01 data logger and the Amp & LPF. Figure 4 shows an example calibration of the magnetic channels checking the sensitivity, linearity, and error. The average sensitivity is 655,968.5 counts/V with a maximum error smaller than 1.35%. Figure 5 shows an example calibration of the electric channels checking the sensitivity, linearity, and error. The average sensitivity is 135,856,047.8 counts/V with a maximum error smaller than 0.8%. Figure 6 shows an example calibration of the tiltmeter channels checking the sensitivity, linearity, and error. The average sensitivity is 1,677,710.6 counts/V with a maximum error smaller than 0.25%.

4.3 Evaluation of the current consumption

The power supplies of the OBEM consist of two 7.2-V battery packs in a series connection with two 3.6-V lithium batteries. One battery pack is for the data logger and converts to ±5 VDC and +3.3 VDC. The other pack is for the sensors and converts to ±5 VDC and +12.0 VDC. Two +7.4-VDC output current batteries were measured for their current consumption measurement using two ammeters connecting the two +7.4-V battery packs. Table 4 shows the current consumption of the OBEM system. The maximum current consumptions of the data logger and sensors are 32 mA and 105 mA, respectively. The total power consumption is less than 1 W, which corresponds to expectations.

4.4 Evaluation of the electrodes

Two pairs of silver chloride electrodes are used for the OBEM. We first put a pair of electrodes separated by a fixed distance within a tank filled with seawater to check the status of the electrodes. Second, we measured the electrical potential and impedance of the electrodes using a digital volt-ohm-milliammeter (VOM) (Fig. 7). Third, we sent a sweep sine signal to check the frequency responses of the electrodes, as shown in Fig. 8. Fourth, we input a DC voltage to check the electrode-induced voltages, as shown in Fig. 9. Table 5 shows the self-potential, impedance, and induced voltages for each pair of electrodes. The ranges of the self-potential and impedance are 0.26–3.63 mV and 243–370 Ω, respectively. The electrical potential shows that 81–167 mV was transmitted from the 5 VDC of the two copper electrodes.

4.5 Evaluation of the fluxgate

The fluxgate is mounted in the sensor ball of the OBEM. Therefore, we could only calculate the total magnetic field (TMF) (Eq. (6)) measured from the three components of the fluxgate. We then compared the difference between the TMF of the OBEM and geomagnetic data of the geophysical database management system from the Central Weather Bureau. The TMF is calculated by

Geosci. Instrum. Method. Data Syst. Discuss., https://doi.org/10.5194/gi-2019-13
Manuscript under review for journal Geosci. Instrum. Method. Data Syst.
Discussion started: 8 May 2019

Geoscientific Instrumentation Methods and Data Systems Discussions
Open Access

$$M_T = \sqrt{(M_X^2 + M_Y^2 + M_Z^2)}, (6)$$

where M_X, M_Y, and M_Z are the components of the north–south, east–west, and vertical magnetic fields, respectively.

4.6 Evaluation of the acoustic transceiver and its transducer

We selected the large-scale Breeze Canal in New Taipei City for testing because it has few obstacles and is suitable for evaluating the functions of the 8011M. The Breeze Canal has a length of approximately 800 m and is located in a straight river with a depth of 2–5 m. The distance between the transducer and the acoustic transceiver was approximately 630 m, and the layout for the field test is shown in Fig. 10. The testing procedure for the transducers is described below. The results are listed in Table 6.

1. Connect the tested transducer and acoustic transceiver via an underwater cable, and place the tested transducer and transceiver at an underwater depth of 1 m.
2. Record the serial numbers of the transducers in a notebook.
3. Send the “ENABLE” command via the 8011M, and then count the response beeps.
4. Send the “RANGE” command via the 8011M five times, and record the distance of each ranging.
5. Send the “DISABLE” command via the 8011M, and then count the response beeps.
6. Replace the transducer, and return to step 2 to repeat the evaluation.

We then checked the acoustic transceivers after all of the transducers were successfully checked; the testing procedure for the acoustic controller is described below. The results are listed in Table 7.

1. Change the acoustic controller, and record its serial number in a notebook.
2. Send the “ENABLE” command via the 8011M, and then count the response beeps.
3. Send the “RANGE” command via the 8011M five times, and record the distance of each ranging.
4. Send the "RELEASE1" command via the 8011M, and then count the response beeps. Check the voltage between Pin1 and Pin2 of JP2 using a VOM. It should

Geosci. Instrum. Method. Data Syst. Discuss., https://doi.org/10.5194/gi-2019-13
Manuscript under review for journal Geosci. Instrum. Method. Data Syst.
Discussion started: 8 May 2019

Geoscientific Instrumentation Methods and Data Systems Discussions
Open Access

be greater than 12.0 VDC.

5. Send the "OPTION1" command via the 8011M, and then count the response beeps. Check the voltage between Pin1 and Pin2 of JP2 using a VOM. It should be 0 VDC.
6. Send the "RELEASE2" command via the 8011M, and then count the response beeps. Check the voltage between Pin3 and Pin4 of JP2 using a VOM. It should be greater than 12.0 VDC.
7. Send the "OPTION1" command via the 8011M, and then count the response beeps. Check the voltage between Pin3 and Pin4 of JP2 using a VOM. It should be 0 VDC.
8. Send the "DISABLE" command via the 8011M, and then count the response beeps.
9. Send the "RANGE" command via the 8011M; there should be no response from the transceiver.
10. Return to step 1 to repeat the evaluation.

A mercury switch is mounted on the transceiver which when turned off responds with 15 beeps and when turned on responds with seven beeps.

5. The preliminary result of the OBEM offshore Taiwan

We deployed six broadband BBYBs and one OBEM near a small submarine volcano area in the OT offshore NE Taiwan (Fig. 11) on 03/26/2018 for a submarine observation to evaluate all the OBEM units. All the equipment was successfully recovered after one month of deployment. Figure 12 shows the time series data of OBEM01. The TMF calculated from the three components of the magnetic field varied in the range of 44,100–4,4150 nT, which corresponded to the geomagnetic field measured by proton magnetometers in Taiwan. The two horizontal magnetic fields contained significant daily variations. Furthermore, the vibrations of the inclinations were significantly affected by two earthquakes on 04/27/2018 (at 12:41 UTC and 12:47 UTC) consistent with seismic signals of the BBYBs (Fig. 13). The average magnetic fields of HX, HY, HZ, and TMF 2 s prior to the earthquakes (12:41 UTC) were 12,900 nT, 34,300 nT, 24,600 nT, and 44137 nT, respectively, the average potential fields of EX and EY were −0.79 mV and −0.149 mV, respectively, and the inclinations of TX and TY were −2.65°

and 1.21°, respectively. These were the averages of the background without earthquakes.

We subtracted the background averages of the magnetic fields and the inclinations to compare the differential during the 12:41 UTC event as shown in Fig. 14. The peak ground motion velocity (PGV) was 2.63 cm s^{-1} on the SH1 corresponding to inclinations of 0.4° and 0.6° for TX and TY with a 100 nT disturbance of HY. There was an insignificant amount of variation in the electric fields. The result shows that the earthquake significantly affected the HY component.

6. Conclusions

A long-period OBEM acquisition platform to measure magnetic and electrical fields on the seafloor was successfully constructed and evaluated by the OBS R&D team for deployment offshore Taiwan. The power consumption of the OBEM is less than 1 W, which means that the lifetime could be extended up to 300 days with the installation of 108 lithium batteries. We deployed and recovered the OBEM at an underwater depth of 1,400 m to acquire the first marine magnetotelluric data offshore NE Taiwan.

Six broadband BBYBs and one OBEM were deployed near a small submarine volcano area offshore NE Taiwan. The TMF calculated from the three magnetic field components varied in the range of 44,100–4,4150 nT, which corresponded to the proton magnetometer measurements of the geomagnetic field in Taiwan. The two horizontal magnetic fields displayed significant daily variations, and the vibrations of the inclinations were significantly affected by the two earthquakes that occurred during the observations. There was an insignificant amount of variation in the electric fields.

Localized micro-earthquakes affected the disturbances of magnetic field and inclinations in this study. Therefore, to improve the efficacy of marine geophysical explorations, a platform for multiple underwater measurements is required including an ocean bottom flow meter, thermometer, and absolute pressure gage. We will focus on such developments in the future.

Acknowledgments

We greatly appreciate the crews of R/V OR2 for the field experiments. The authors

Geosci. Instrum. Method. Data Syst. Discuss., https://doi.org/10.5194/gi-2019-13
Manuscript under review for journal Geosci. Instrum. Method. Data Syst.
Discussion started: 8 May 2019

Geoscientific Instrumentation Methods and Data Systems Discussions

acknowledge the financial support from the Ministry of Science and Technology of Taiwan under grant numbers of 105-2116-M-019-001, 106-2116-M-001-008, 106-2116-M-019-003, and 107-2116-M-019-006. We also thank four years of the Taiwan-German cooperative projects on gas hydrate of NEPII for supporting the funds of the instrument deployment of the OBEMs. We would like to thank the TEC Data Center for proving graphical services.

References

Bertrand, E., Unsworth, M., Chiang, C. W., Chen, C. S., Chen, C. C., Wu, F., Turkoglu, E., Hsu, H. L., and Hill, G.: Magnetotelluric evidence for thick-skinned tectonics in central Taiwan, Geology, 37, 711-714, 2009.

Bertrand, E. A., Unsworth, M. J., Chiang, C. W., Chen, C. S., Chen, C. C., Wu, F. T., Turkoglu, E., Hsu, H. L., and Hill, G. J.: Magnetotelluric imaging beneath the Taiwan orogen: An arc-continent collision, J Geophys Res-Sol Ea, 117, 2012.

Chiang, C. W., Chen, C. C., Unsworth, M., Bertrand, E., Chen, C. S., Kieu, T. D., and Hsu, H. L.: The deep electrical structure of southern Taiwan and its tectonic implications (vol 21, pg 879, 2010), Terr. Atmos. Ocean Sci., 22, 371-371, 2011a.

Chiang, C. W., Chen, C. C., Unsworth, M., Bertrand, E., Chen, C. S., Thong, D. K., and Hsu, H. L.: The deep electrical structure of southern Taiwan and its Tectonic Implications, Terr. Atmos. Ocean Sci., 21, 879-895, 2010.

Chiang, C. W., Goto, T., Mikada, H., Chen, C. C., and Hsu, S. K.: Sensitivity of deep-towed marine electrical resistivity imaging using two-dimensional inversion: a case study on methane hydrate, Terr. Atmos. Ocean Sci., 23, 725-732, 2012.

Chiang, C. W., Goto, T. N., Chen, C. C., and Hsu, S. K.: Efficiency of a marine towed electrical resistivity method, Terr. Atmos. Ocean Sci., 22, 443-446, 2011b.

Chiang, C. W., Hsu, H. L., and Chen, C. C.: An investigation of the 3D electrical resistivity structure in the Chingshui geothermal area, NE Taiwan, Terr. Atmos. Ocean Sci., 26, 269-281, 2015.

Chiang, C. W., Unsworth, M. J., Chen, C. S., Chen, C. C., Lin, A. T. S., and Hsu, H. L.: Fault zone resistivity structure and monitoring at the Taiwan Chelungpu Drilling Project (TCDP), Terr. Atmos. Ocean Sci., 19, 473-479, 2008.

Constable, S.: Ten years of marine CSEM for hydrocarbon exploration, Geophysics, 75, A67-A81, 2010.

Geoscientific Instrumentation Methods and Data Systems
Discussions

Ellis, M., Evans, R. L., Hutchinson, D., Hart, P., Gardner, J., and Hagen, R.: Electromagnetic surveying of seafloor mounds in the northern Gulf of Mexico, Mar. Pet. Geol., 25, 960-968, 2008.

Evans, R. L., Hirth, G., Baba, K., Forsyth, D., Chave, A., and Mackie, R.: Geophysical evidence from the MELT area for compositional controls on oceanic plates, Nature, 437, 249-252, 2005.

Goto, T. N., Kasaya, T., Machiyama, H., Takagi, R., Matsumoto, R., Okuda, Y., Satoh, M., Watanabe, T., Seama, N., Mikada, H., Sanada, Y., and Kinoshita, M.: A marine deep-towed DC resistivity survey in a methane hydrate area, Japan Sea, Explor. Geophys., 39, 52-59, 2008.

Hsu, S. K., Chiang, C. W., Evans, R. L., Chen, C. S., Chiu, S. D., Ma, Y. F., Chen, S. C., Tsai, C. H., Lin, S. S., and Wang, Y. S.: Marine controlled source electromagnetic method used for the gas hydrate investigation in the offshore area of SW Taiwan, J. Asian Earth Sci., 92, 224-232, 2014.

Kasaya, T. and Goto, T.: A small ocean bottom electromagnetometer and ocean bottom electrometer system with an arm-folding mechanism, Explor. Geophys., 40, 41-48, 2009.

Key, K.: Marine Electromagnetic Studies of Seafloor Resources and Tectonics, Surv. Geophys., 33, 135-167, 2012.

Kuo, B. Y., Crawford, W. C., Webb, S. C., Lin, C. R., Yu, T. C., and Chen, L. W.: Faulting and hydration of the upper crust of the SW Okinawa Trough during continental rifting: Evidence from seafloor compliance inversion, Geophys. Res. Lett., 42, 4809-4815, 2015.

Kuo, B. Y., Wang, C. C., Lin, S. C., Lin, C. R., Chen, P. C., Jang, J. P., and Chang, H. K.: Shear-wave splitting at the edge of the Ryukyu subduction zone, Earth Planet. Sci. Lett., 355, 262-270, 2012.

Kuo, B. Y., Webb, S. C., Lin, C. R., Liang, W. T., and Hsiao, N. C.: Removing infragravity-wave-induced noise from Ocean-Bottom Seismographs (OBS) data deployed offshore of Taiwan, Bull. Seismol. Soc. Am., 104, 1674-1684, 2014.

Schwalenberg, K., Rippe, D., Koch, S., and Scholl, C.: Marine-controlled source electromagnetic study of methane seeps and gas hydrates at Opouawe Bank, Hikurangi Margin, New Zealand, J Geophys Res-Sol Ea, 122, 3334-3350, 2017.

Utada, H.: Electromagnetic exploration of the oceanic mantle, P Jpn Acad B-Phys, 91, 203-222, 2015.

Weitemeyer, K. A., Constable, S., and Trehu, A. M.: A marine electromagnetic survey to detect gas hydrate at Hydrate Ridge, Oregon, Geophys. J. Int., 187, 45-62, 2011.

Weitemeyer, K. A., Constable, S. C., Key, K. W., and Behrens, J. P.: First results from a marine controlled-source electromagnetic survey to detect gas hydrates offshore Oregon, Geophys. Res. Lett., 33, 2006.

TABLE AND FIGURE CAPTIONS

Table 1. The OBEM01 data logger calibration of the magnetic channels with Amp & LPF: the background noise, sensitivity, linearity error, and dynamic range.

Table 2. The OBEM01 data logger calibration of the electric channels with Amp & LPF: the background noise, sensitivity, linearity error, and dynamic range.

Table 3. The OBEM01 data logger calibration of the tiltmeter channels with Amp & LPF: the background noise, sensitivity, linearity error, and dynamic range.

Table 4. The total current consumption of the OBEMs.

Table 5. The self-potential, impedance, and induced voltage results for each pair of silver chloride electrodes.

Table 6. Example results for the functional test of the acoustic transducer.

Table 7. Example results for the functional test of the acoustic controller.

Figure 1. A block diagram of the OBEM. The inputs of the two electric fields, two inclinations, and three magnetic fields pass through the Amp & LPF in the data logger, which contains a 64-GB SD card. The SeaSCAN time base module is integrated into the data logger and has a timing error smaller than 3 s y^{-1}. The EdgeTech acoustic transceiver and transducer are used for the positioning and releasing of the anchor. The radio and flash beacons are used to locate the OBEM at the sea surface during recovery operations.

Figure 2. A block diagram of the OBEM data logger. The ADS1278EVM is a 24-bit A/D with eight inputs used for converting analog signals via the amplifier and low-pass filter (Amp & LPF) to digital data. The Amp & LPF adjusts the output voltages of the sensors of the fluxgate, tiltmeter, and electric receivers to suitable A/D input levels. The two MCUs of the MPS430F5436A process the timing synchronization by the

Geosci. Instrum. Method. Data Syst. Discuss., https://doi.org/10.5194/gi-2019-13
Manuscript under review for journal Geosci. Instrum. Method. Data Syst.
Discussion started: 8 May 2019

Geoscientific Instrumentation Methods and Data Systems Discussions
Open Access

SeaSCAN of time base and GPS modules, the digital data storage to the SD card with a standard SDHC, and the user interface communication with a PC.

Figure 3. A photograph of the OBEM01 and its specific modules.

Figure 4. Calibration results for the magnetic channels of the OBEM01. The average sensitivity is 655,968.5 counts/V, and the maximum error is <1.35%.

Figure 5. Calibration results for the electric channels of the OBEM01. The average sensitivity is 1,358,568,047.8 counts/V, and the maximum error is <0.8%.

Figure 6. Calibration results for the inclination channels of the OBEM01. The average sensitivity is 1,677,710.6 counts/V, and the maximum error is <0.25%.

Figure 7. The layout for the evaluation of the electric receivers. Two copper electrodes are used to vary the input signals. A pair of silver chloride electrodes are placed at the corner of a tank with an area of 68 cm × 49 cm filled with 15 cm of seawater. A VOM is used to measure the self-potential and impedance of the electrodes.

Figure 8. The responses of the electrodes with varying frequencies. The response curves of V_o/V_i are proportional to the frequency on a log scale.

Figure 9. The responses of the electrodes with varying voltages. The input was ranged from 500 mVDC to 2,500 mVDC to check the induced voltage; the induced voltages are proportional to the input voltages.

Figure 10. A map of the field test to evaluate the acoustic transducer, acoustic controller, and 8011M.

Figure 11. A location map showing the BBYBs and OBEM with triangle and diamond symbols, respectively.

Figure 12. The OBEM01 time series data. The panels from top to bottom in the figure show the four magnetic fields: TMF, HX, HY, and HZ, the two electric fields: EX and EY, and the two inclinations: TX and TY.

Figure 13. Comparison of the OBEM01 and 1802OBS time series data during the two earthquakes. The two earthquakes affected the inclinations. The first and secondary earthquakes occurred at 12:41 UTC and 12:47 UTC, respectively, on 04/27/2018.

Figure 14. The variations in PGV, TMF, HY, TX, and TY during the first earthquake. The PGV of 2.63 cm/s affected the inclinations by 0.601° and 0.404° for TX and TY, respectively, and the HY magnetic field had a peak of 100 nT.

TABLES AND FIGURES

Table 1

input (V)	output(MX)	remove offset(MX)	output(MY)	remove offset(MY)	output(MZ)	remove offset(MZ)	input	sensitivity(MX)	error%(MX)	sensitivity(MY)	error%(MY)	sensitivity(MZ)	error%(MZ)
-10.0	-6471112.3	-6474180.3	-6472546.0	-6471775.5	-6476434.0	-6472369.2	-10.0	647418.03	-1.322	647177.55	-1.342	647236.92	-1.311
-9.0	-5869208.1	-5872276.1	-5871019.8	-5870249.3	-5874491.2	-5870426.4	-9.0	652475.12	-0.551	652249.92	-0.568	652269.60	-0.543
-8.0	-5249375.0	-5252443.1	-5251749.3	-5250978.8	-5254300.4	-5250235.6	-8.0	656555.38	0.070	656372.35	0.060	656279.45	0.068
-7.0	-4600873.9	-4603941.9	-4603731.6	-4602961.1	-4605554.6	-4601489.8	-7.0	657705.99	0.246	657565.87	0.242	657355.68	0.232
-6.0	-3943651.8	-3946719.8	-3946684.9	-3945914.4	-3948745.5	-3944680.7	-6.0	657786.64	0.258	657652.39	0.255	657446.78	0.246
-5.0	-3285800.0	-3288868.0	-3289015.6	-3288245.1	-3291209.9	-3287145.1	-5.0	657773.61	0.256	657649.02	0.255	657429.02	0.243
-4.0	-2628274.7	-2631342.8	-2631609.2	-2630838.7	-2634025.5	-2629960.7	-4.0	657835.69	0.266	657709.67	0.264	657490.16	0.253
-3.0	-1970402.2	-1973470.2	-1973864.9	-1973094.4	-1976483.5	-1972418.7	-3.0	657823.41	0.264	657698.14	0.262	657472.91	0.250
-2.0	-1312631.3	-1315699.4	-1316216.6	-1315446.1	-1319057.9	-1314993.0	-2.0	657849.68	0.268	657723.04	0.266	657496.52	0.254
-1.0	-654832.3	-657900.3	-658536.9	-657766.4	-661600.3	-657535.4	-1.0	657900.33	0.275	657766.39	0.273	657535.43	0.260
0.0	3068.0	0.0	-770.5	0.0	-4064.8	0.0	1.0	657880.86	0.272	657759.33	0.271	657535.67	0.260
0.0	3018.0	0.0	-810.1	0.0	-4118.9	0.0	2.0	657859.96	0.269	657741.27	0.269	657504.87	0.255
1.0	660948.9	657930.8	656988.8	657798.9	653470.8	657589.8	3.0	657837.12	0.266	657727.37	0.267	657491.44	0.253
2.0	1318787.9	1315769.9	1314712.0	1315522.1	1310944.9	1315063.8	4.0	657859.68	0.269	657747.51	0.270	657499.55	0.254
3.0	1976579.4	1973561.4	1972411.6	1973221.7	1968409.5	1972528.4	5.0	657811.97	0.262	657692.96	0.261	657443.49	0.245
4.0	2634506.8	2631488.7	2630219.5	2631029.6	2625933.4	2630052.3	6.0	657832.48	0.265	657705.29	0.263	657459.85	0.248
5.0	3292127.9	3289109.8	3287694.3	3288504.4	3283152.6	3287271.6	7.0	657688.48	0.243	657584.21	0.245	657397.26	0.238
6.0	3950062.9	3947044.9	3945461.2	3946271.3	3940694.3	3944813.2	8.0	656372.97	0.043	656448.69	0.072	656415.89	0.089
7.0	4606887.4	4603869.3	4602318.9	4603129.0	4597716.0	4601834.9	9.0	652314.56	-0.576	652334.15	-0.556	652469.16	-0.513
8.0	5254051.8	5251033.8	5250819.0	5251629.1	5247262.3	5251381.2	10.0	647283.74	-1.343	647270.99	-1.327	647438.99	-1.280
9.0	5873899.1	5870881.0	5870236.8	5871046.9	5868157.6	5872276.5	Average	656093.29		655978.81		655833.43	
10.0	6475905.4	6472887.3	6471939.4	6472749.5	6470325.1	6474444.0	**Average sensitivity 655968.51**						

Geosci. Instrum. Method. Data Syst. Discuss., https://doi.org/10.5194/gi-2019-13
Manuscript under review for journal Geosci. Instrum. Method. Data Syst.
Discussion started: 8 May 2019

Geoscientific Instrumentation Methods and Data Systems
Discussions
Open Access

Table 2

Input (V)	Output (EX)	remove offset (EX)	Output (EY)	remove offset (EY)	input (V)	sensitivity (EX)	error%(EX)	sensitivity (EY)	error% (EY)
-0.0060	-7973544.4	-8134716.5	-8135152.5	-8127780.7	-0.0060	1355786076.8	-0.186	1354630119.94	-0.413
-0.0050	-6611209.2	-6772381.3	-6778699.0	-6771327.2	-0.0050	1354476260.4	-0.283	1354265449.87	-0.439
-0.0040	-5257318.1	-5418490.2	-5459462.4	-5452090.6	-0.0040	1354622556.8	-0.272	1363022659.48	0.204
-0.0030	-3909730.8	-4070902.9	-4084816.3	-4077444.6	-0.0030	1356967645.6	-0.099	1359148194.55	-0.081
-0.0020	-2558460.2	-2719632.3	-2729127.4	-2721755.7	-0.0020	1359816155.1	0.110	1360877857.04	0.047
-0.0010	-1207366.1	-1368538.2	-1376888.8	-1369517.1	-0.0010	1368538175.4	0.753	1369517055.70	0.682
0.0000	161172.1	0.0	-7371.7	0.0	0.0010	1368374397.6	0.740	1368868765.94	0.634
0.0000	95647.7	0.0	-86742.8	0.0	0.0020	1359089788.7	0.057	1361166374.27	0.068
0.0010	1464022.1	1368374.4	1282126.0	1368868.8	0.0030	1357537440.6	-0.057	1359385875.47	-0.063
0.0020	2813827.3	2718179.6	2635589.9	2722332.7	0.0040	1354770300.9	-0.261	1351072742.78	-0.674
0.0030	4168260.1	4072612.3	3991414.8	4078157.6	0.0050	1354197292.1	-0.303	1349041143.00	-0.824
0.0040	5514728.9	5419081.2	5317548.2	5404291.0	0.0060	1355623271.0	-0.198	1354837547.58	-0.397
0.0050	6866634.2	6770986.5	6658462.9	6745205.7	Average	1358316613.4		1358819482.1	
0.0060	8229387.4	8133739.6	8042282.5	8129025.3	**Average sensitivity 1358568047.8**				

Table 3

input(V)	output(TX)	remove offset(TX)	output(TY)	remove offset(TY)	input	sensitivity(TX)	error%(TX)	sensitivity(TY)	error%(TY)
-5.00	-8387520.5	-8386705.4	-8387650.3	-8386680.2	-5.0	1677341.1	-0.016	1677336.04	-0.029
-4.00	-6712516.4	-6711701.2	-6712951.5	-6711981.4	-4.0	1677925.3	0.019	1677995.36	0.011
-3.00	-5034477.1	-5033661.9	-5034843.7	-5033873.6	-3.0	1677887.3	0.017	1677957.86	0.008
-2.00	-3356824.4	-3356009.2	-3357098.5	-3356128.4	-2.0	1678004.6	0.024	1678064.22	0.015
-1.00	-1678971.4	-1678156.3	-1679215.6	-1678245.5	-1.0	1678156.3	0.033	1678245.46	0.026
0.00	-815.2	0.0	-970.1	0.0	1.0	1678289.0	0.041	1678377.40	0.033
0.00	-902.3	0.0	-1060.3	0.0	2.0	1678208.8	0.036	1678269.99	0.027
1.00	1677386.7	1678289.0	1677317.1	1678377.4	3.0	1678386.2	0.047	1678923.87	0.066
2.00	3355515.3	3356417.6	3355479.6	3356540.0	4.0	1678457.5	0.051	1679001.78	0.071
3.00	5034256.3	5035158.6	5035711.3	5036771.6	5.0	1673403.6	-0.250	1673981.58	-0.228
4.00	6712927.8	6713830.2	6714946.8	6716007.1	Average	1677606.0		1677815.36	
5.00	8366115.7	8367018.0	8368847.6	8369907.9	**Average sensitivity**			**1677710.6**	

Table 4

Logger S/N	Turn-on Mode (mA)			Recording Mode (mA)		
	7.2V for Data logger	7.2V for Sensors	Power consumption	7.2V for Data logger	7.2V for Sensors	Power consumption
OBEM01	32	104	0.98	31	105	0.98
OBEM02	30	94	0.89	29	97	0.91
OBEM03	29	103	0.95	29	104	0.96

Geosci. Instrum. Method. Data Syst. Discuss., https://doi.org/10.5194/gi-2019-13
Manuscript under review for journal Geosci. Instrum. Method. Data Syst.
Discussion started: 8 May 2019

Geoscientific Instrumentation Methods and Data Systems Discussions
Open Access

Table 5

	Electrical potential	Impedance	Input DC5V, induce voltage
OBEM01(EX)	0.56 mV	245 Ω	164 mV
OBEM01(EY)	0.26 mV	272 Ω	167 mV
OBEM02(EX)	3.63 mV	243 Ω	81 mV
OBEM02(EY)	1.93 mV	370 Ω	95 mV
OBEM03(EX)	2.38 mV	267 Ω	83 mV
OBEM03(EY)	2.1 mV	331 Ω	83 mV

Table 6

Transducer S/N	Enable Beep (Times)	Disable Beep (Times)	1st Ranging Distance show on 8011M (m)	2nd Ranging Distance show on 8011M (m)	3rd Ranging Distance show on 8011M (m)	4th Ranging Distance show on 8011M (m)	5th Ranging Distance show on 8011M (m)	Judgment
35427	15	15	629	628	630	627	628	Good
35428	15	15	629	627	629	630	629	Good
35429	15	15	630	630	630	629	629	Good

Table 7

S/N	Enable Beep (Times)	1st Ranging Distance show on 8011M (m)	2nd Ranging Distance show on 8011M (m)	3rd Ranging Distance show on 8011M (m)	4th Ranging Distance show on 8011M (m)	5th Ranging Distance show on 8011M (m)	RELEASE1 Beep Times/Volt	OPTION1 Beep (Times)	RELEASE2 Beep Times/Volt	OPTION1 Beep (Times)	DISABLE Beep (Times)
50854	15	628	629	630	630	630	15/ 12.77V	15	15/ 12.77V	15	15
50784	7	629	630	630	630	630	7/ 12.77V	7	7/ 12.77V	7	7
50783	15	628	628	628	629	631	15/ 12.77V	15	15/ 12.77V	15	15

Geosci. Instrum. Method. Data Syst. Discuss., https://doi.org/10.5194/gi-2019-13
Manuscript under review for journal Geosci. Instrum. Method. Data Syst.
Discussion started: 8 May 2019

Geoscientific Instrumentation Methods and Data Systems
Open Access
Discussions

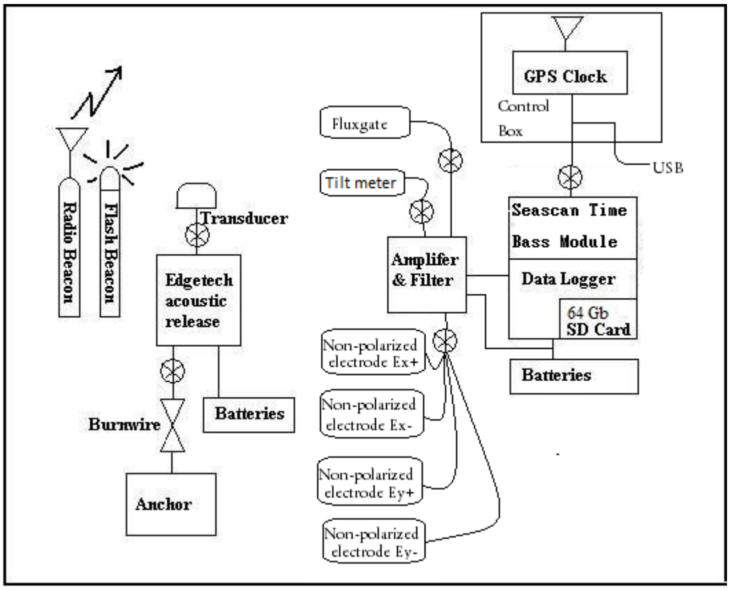

Figure 1

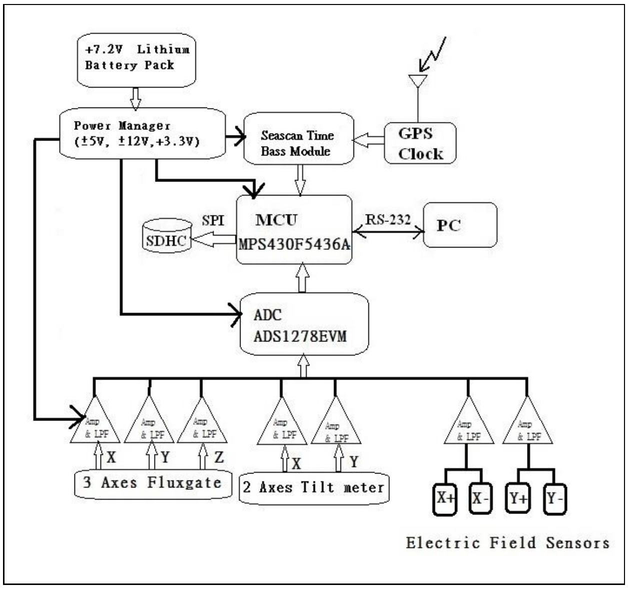

Figure 2

Geosci. Instrum. Method. Data Syst. Discuss., https://doi.org/10.5194/gi-2019-13
Manuscript under review for journal Geosci. Instrum. Method. Data Syst.
Discussion started: 8 May 2019

Geoscientific Instrumentation Methods and Data Systems
Open Access
Discussions

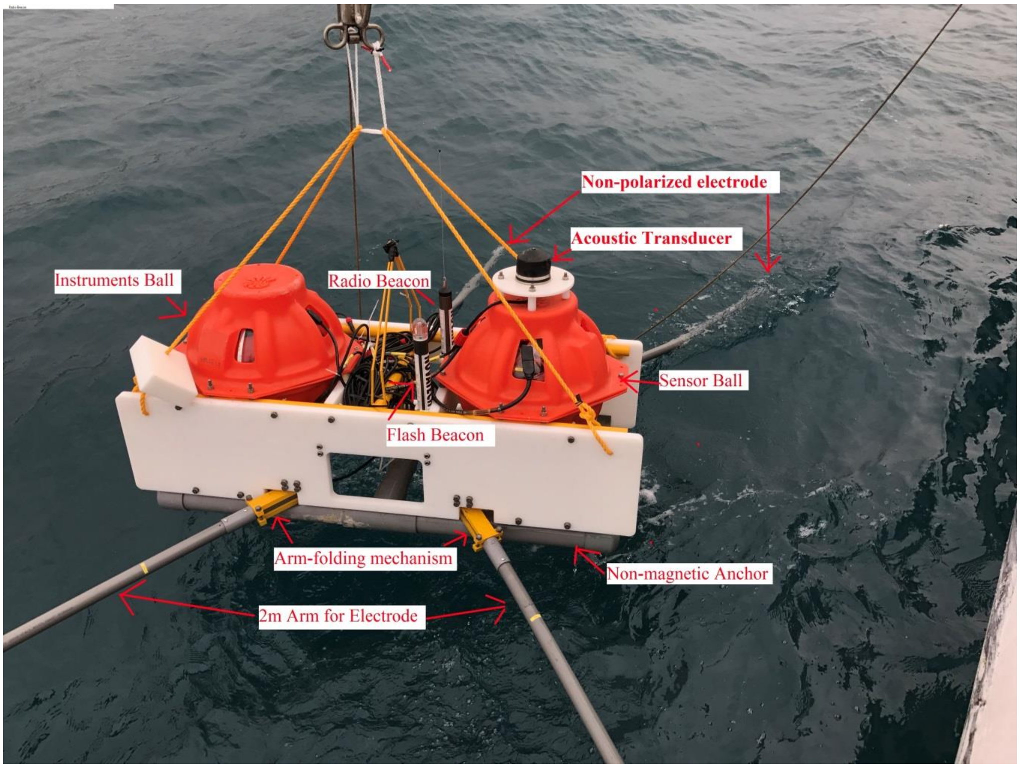

Figure 3

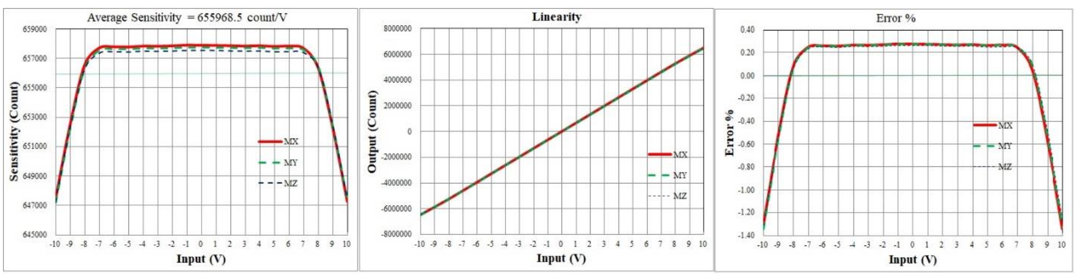

Figure 4

Geosci. Instrum. Method. Data Syst. Discuss., https://doi.org/10.5194/gi-2019-13
Manuscript under review for journal Geosci. Instrum. Method. Data Syst.
Discussion started: 8 May 2019

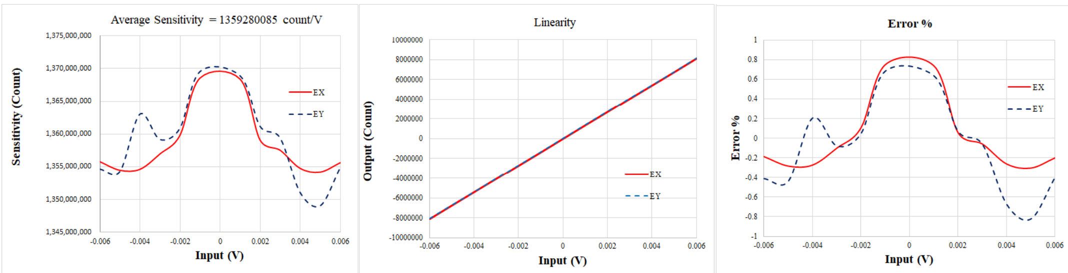

Figure 5

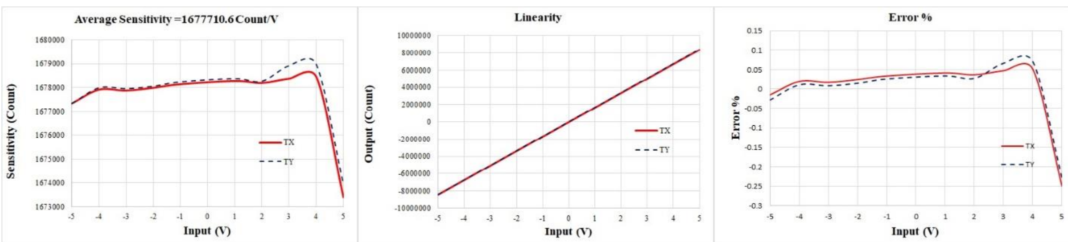

Figure 6

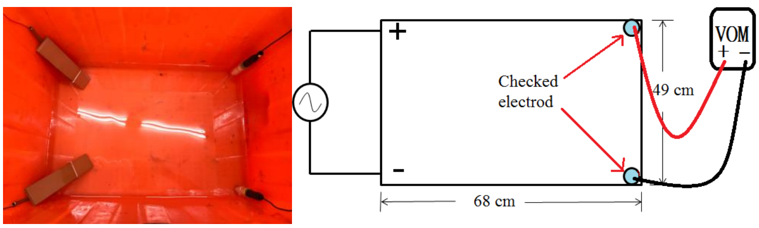

Figure 7

Geosci. Instrum. Method. Data Syst. Discuss., https://doi.org/10.5194/gi-2019-13
Manuscript under review for journal Geosci. Instrum. Method. Data Syst.
Discussion started: 8 May 2019

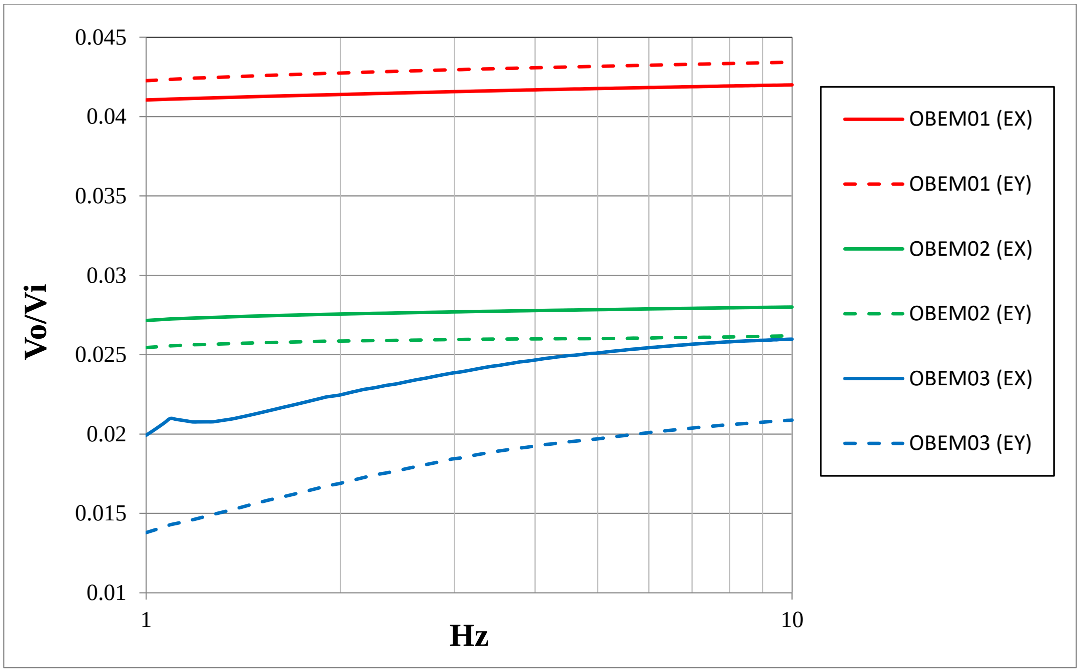

Figure 8

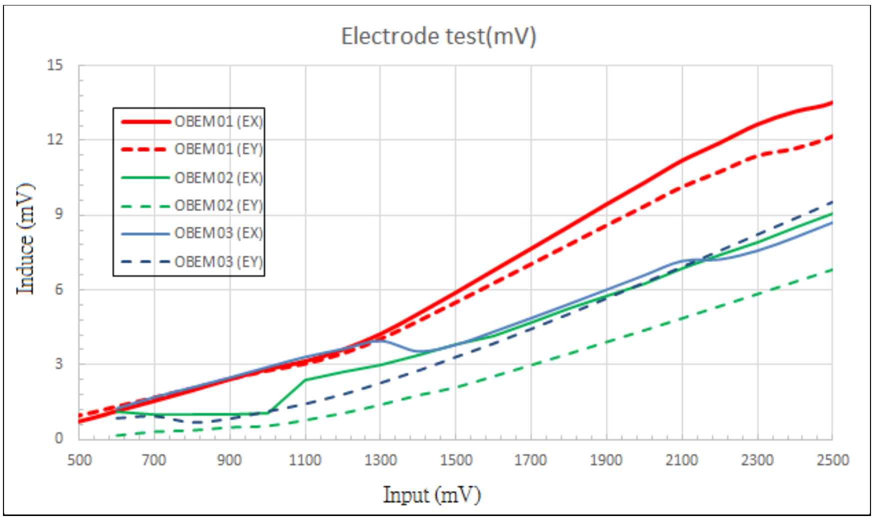

Figure 9

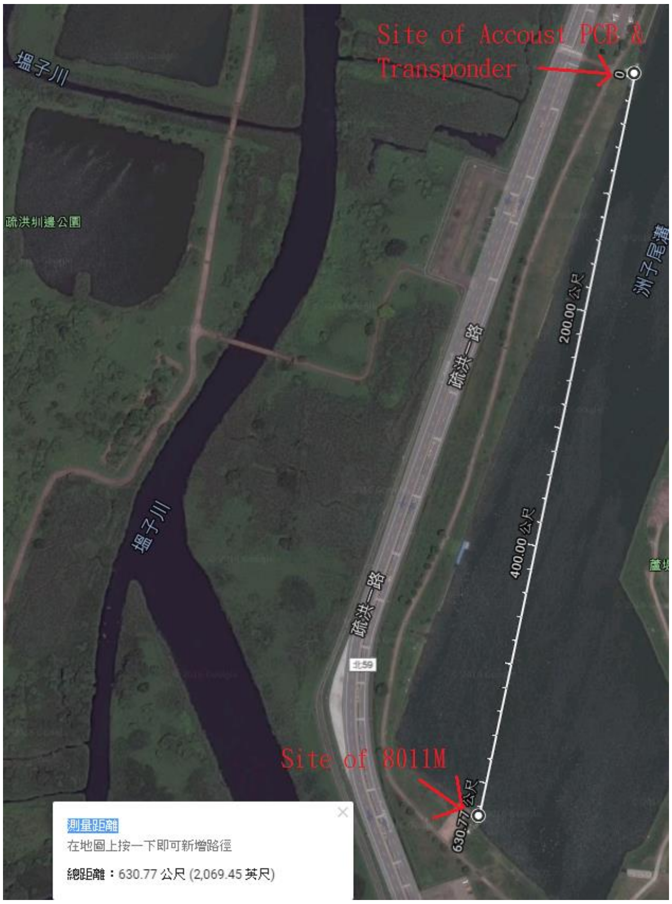
Site of Accoust PCB &
Transponder
0
Site of 8011M
埤子川
疏洪圳邊公園
疏洪一路
洲子尾濱
200.00 公尺
400.00 公尺
630.77 公尺
北59
測量距離
在地圖上按一下即可新增路徑
總距離：630.77 公尺 (2,069.45 英尺)

Figure 10

Geosci. Instrum. Method. Data Syst. Discuss., https://doi.org/10.5194/gi-2019-13
Manuscript under review for journal Geosci. Instrum. Method. Data Syst.
Discussion started: 8 May 2019

Geoscientific Instrumentation Methods and Data Systems
Open Access
Discussions

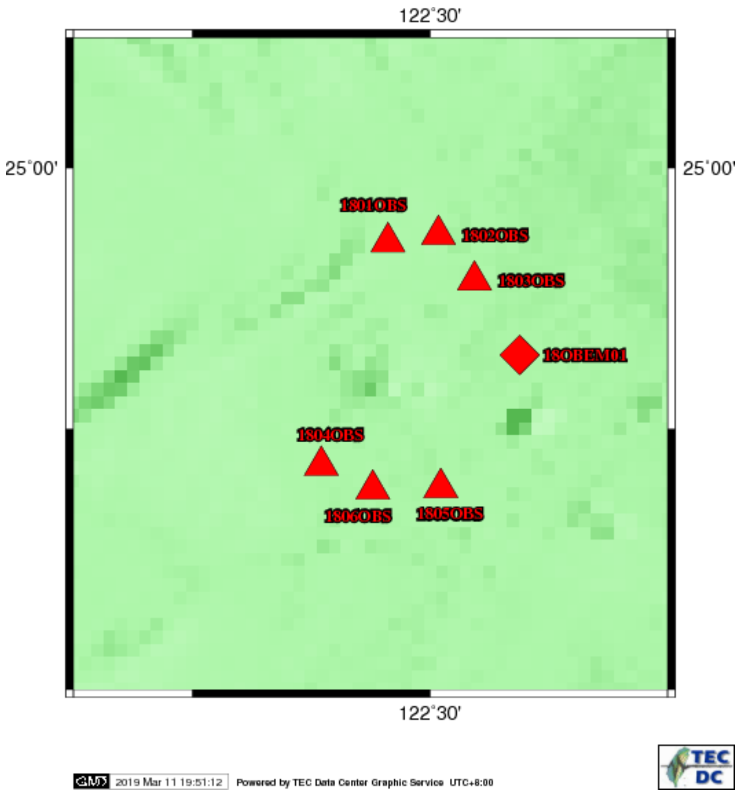

Figure 11

Geosci. Instrum. Method. Data Syst. Discuss., https://doi.org/10.5194/gi-2019-13
Manuscript under review for journal Geosci. Instrum. Method. Data Syst.
Discussion started: 8 May 2019

Geoscientific Instrumentation Methods and Data Systems
Open Access
Discussions

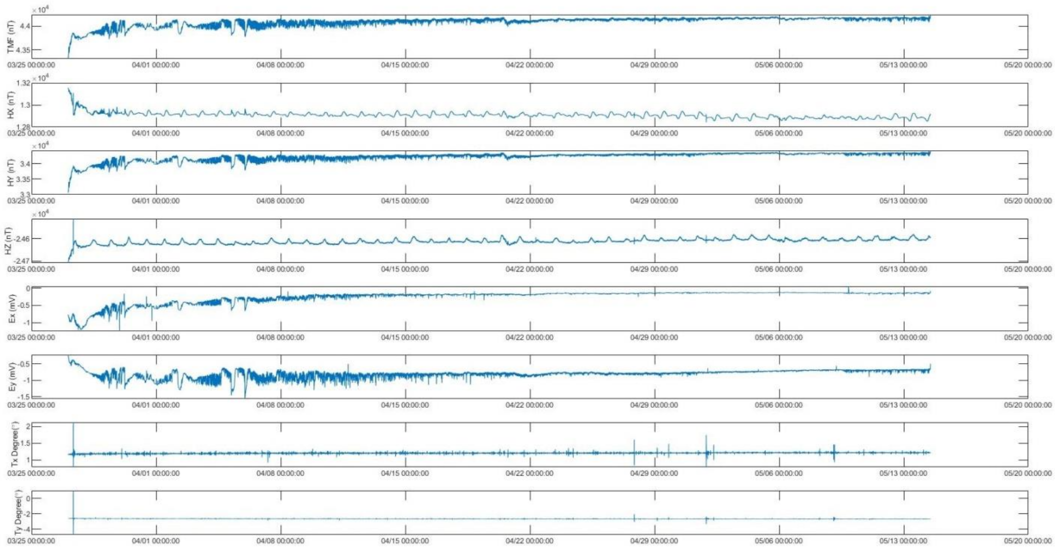

Figure 12

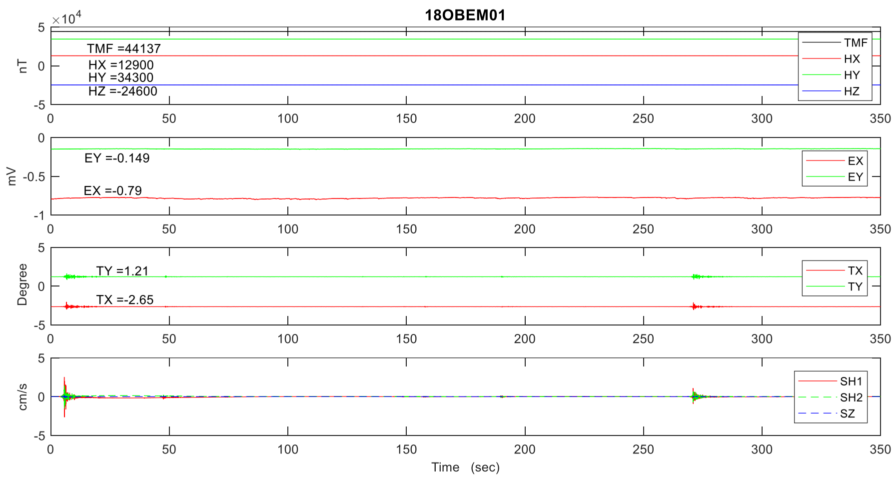

Figure 13

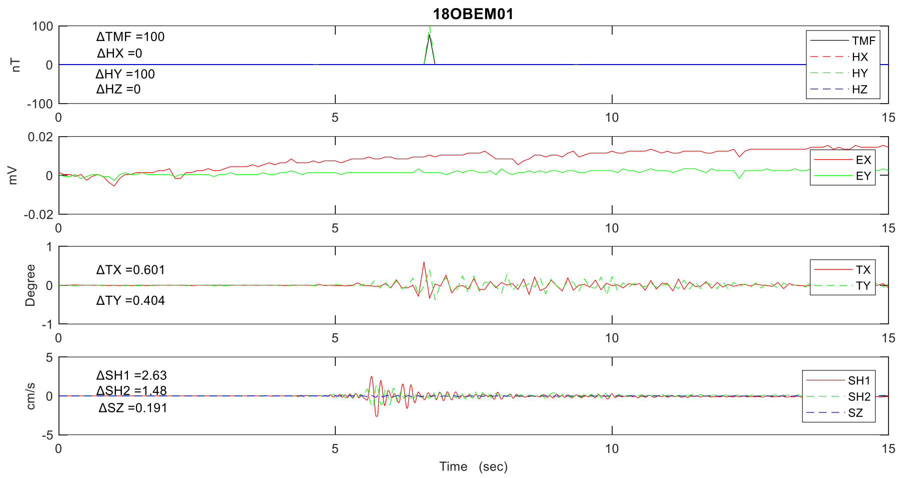
18OBEM01
ΔTMF =100
ΔHX =0
ΔHY =100
ΔHZ =0
TMF
HX
HY
HZ
nT
EX
EY
mV
ΔTX =0.601
ΔTY =0.404
TX
TY
Degree
ΔSH1 =2.63
ΔSH2 =1.48
ΔSZ =0.191
SH1
SH2
SZ
cm/s
Time (sec)

Figure 14